Structure, shape and dynamics of biological membranes.

Idema, T.

CHAPTER 7

TUBE PULLING BY MOLECULAR MOTORS

In cells, membrane tubes are extracted by molecular motors. Although individual motors cannot provide enough force to pull a tube, clusters of such motors can. In this chapter we use a minimal *in vitro* model system to investigate how the tube pulling process depends on fundamental properties of the motor species involved. Previously, it has been shown that processive motors can pull tubes by dynamic association at the tube tip. Remarkably, as was recently shown in experiment, nonprocessive motors can also cooperatively extract tubes. Moreover, the tubes pulled by nonprocessive motors exhibit rich dynamics as compared to those pulled by their processive counterparts. The experiments show distinct phases of persistent growth, retraction and an intermediate regime characterized by highly dynamic switching between the two. We interpret the different phases in the context of a single-species model. The model assumes only a simple motor clustering mechanism along the length of the entire tube and the presence of a length-dependent tube tension. The resulting dynamic distribution of motor clusters acts as both a velocity and distance regulator for the tube. We show the switching phase to be an attractor of the dynamics of this model, suggesting that the switching observed experimentally is a robust characteristic of nonprocessive motors. A similar system could regulate *in vivo* biological membrane networks.

7.1 Introduction

Dynamic interactions between the cell's cytoskeletal components and the lipid membranes that compartmentalize the cell interior are critical for intracellular trafficking. A trademark of these cytoskeletal-membrane interactions is the presence of continuously changing membrane tube networks. In *e.g.* the endoplasmic reticulum *in vivo* [121, 122] and in cell-free extracts [123–126], new membrane tubes are constantly formed while old ones disappear. Colocalization of these membrane tubes with the underlying cytoskeleton has led to the finding that cytoskeletal motor proteins can extract membrane tubes [126]. Motors must work collectively to extract membrane tubes [25,26,127], because the force needed to form a tube, $\mathcal{F}_{\text{tube}}$ [47], is larger than the mechanical stall force of an individual motor [128].

In this chapter we investigate how the tube pulling process depends on fundamental properties of the motors involved. We use two motor proteins from the Kinesin family [129], which walk on microtubules (MTs), the stiffest components of the cytoskeleton. As a model processive motor, we use Kinesin-1 (which we will call Kinesin for convenience), because it is the motor used *in vivo* for transport of vesicles and membrane material towards the plus end of microtubules. These processive Kinesin motors take many steps toward the plus end (to the cell periphery) before unbinding from a microtubule (MT) and have a duty ratio of approximately 1 (fraction of time spent bound to the MT) [130]. The nonprocessive motor we use is nonclaret disjunctional (Ncd), from the Kinesin-14 family, a motor protein which is highly homologous to Kinesin-1, yet fundamentally different biophysically. It is strictly non-processive: motors unbind after a single step [130] characterized by a duty ratio of 0.15 [22]. Both the Kinesin and Ncd motors are unidirectional, but they move in opposite directions. Kinesin moves towards the plus end of the MT (directed towards the plasma membrane), Ncd moves towards the minus end (directed towards the nucleus) [23]. Although Ncd is not involved in tube formation *in vivo*, it is an ideal candidate to study the effect of processivity on the tube pulling process *in vitro* because of its high similarity to Kinesin. Throughout this chapter we will therefore compare the results of pulling experiments with Kinesin and Ncd.

The bulk characteristics of molecular motors which walk on biopolymers like MTs can be studied in gliding assays [130–132]. In a gliding assay the motors are rigidly bound to a glass substrate, in such a way that the walking heads are pointing away from the glass surface. The biopolymers are then deposited on top of the substrate and their motion is followed. Typically the motors are not labeled (and thus invisible), whereas the polymers are tracked by attaching fluorescent molecules to them. Gliding assay experiments are used to measure the walking speeds of molecular motors, as a function of motor density and ATP concentration. In the specific case of Kinesin walking on microtubules, such experiments show a well-defined velocity of about $500\ \mathrm{nm/s}$, indepen-

dent of the motor concentration, which is consistent with the fact that Kinesin is highly processive. The same gliding assay with Ncd motors shows a linear dependence of MT gliding speeds on motor concentration, up to a saturation of $120\ \mathrm{nm/s}$ [133]. The linear dependence of motor concentration is a hallmark of nonprocessivity [130]. Because of their nonprocessive walking behavior, it is not *a priori* obvious that Ncd motors can cooperatively pull membrane tubes.

In the experiments described in this chapter, we study the formation of membrane tube networks pulled from Giant Unilamellar Vesicles (GUVs) by motors walking on immobilized MTs (figure 7.1a, for details see appendix 7.A). The experiments were performed by P. M. Shaklee, who has a joint position at the Leiden experimental biophysics group and at AMOLF in Amsterdam. Earlier experiments showed that using Kinesin in the same setup resulted in the formation of extended membrane tube networks [25, 26]. The key findings of the experiments with Ncd are that Ncd motors readily extract tubes, and that the tubes display more complex dynamics than those pulled by processive motors. We observed the emergence of a distinct switching behavior: the tube alternates between forward and backward movement with variable speeds, ranging from $+120\ \mathrm{nm/s}$ to $-220\ \mathrm{nm/s}$. This bidirectional switching is a phenomenon entirely absent in membrane tubes extracted by processive Kinesin motors, which proceed at constant speeds up to $400\ \mathrm{nm/s}$.

Though the bidirectional tube behavior we observe could result from motors forced to walk backward under tension [24], thus far there is no experimental evidence to support this interpretation for unidirectional motors [134, 135]. Moreover, the retraction speeds are much higher than the maximum speeds measured in Ncd gliding assays so that the reverse powerstroke would have to be much faster than the experimentally found speeds. We suggest a mechanism by which nonprocessive motors form clusters along the length of the entire tube, each of which is capable of withstanding the force due to tube tension. These clusters are dynamic entities containing a fluctuating amount of motors. The motors in the cluster at the tip of the membrane tube pull forward, until the fluctuating cluster size falls below a critical value and the tip cluster can no longer support the tube. We implement this model mathematically and show that its necessary consequence is a distinct switching behavior in membrane tubes extracted from a vesicle under tension. We analyze the experimental results in the context of this model and we predict the distribution of motor clusters all along the length of a membrane tube. The resulting dynamic distribution of motor clusters acts as both a velocity and a distance regulator for the tube. Finally, using simulations, we trace the evolution of the system and find the same bidirectional behavior as observed experimentally. In short, we show that not only can nonprocessive, unidirectional Ncd motors act cooperatively to extract membrane tubes - they do so in a highly dynamic, bidirectional switching fashion. Our findings suggest an alternative explanation for *in vivo* bidirectional tube dynamics, often credited to the presence of a mixture of plus and minus end directed motors.

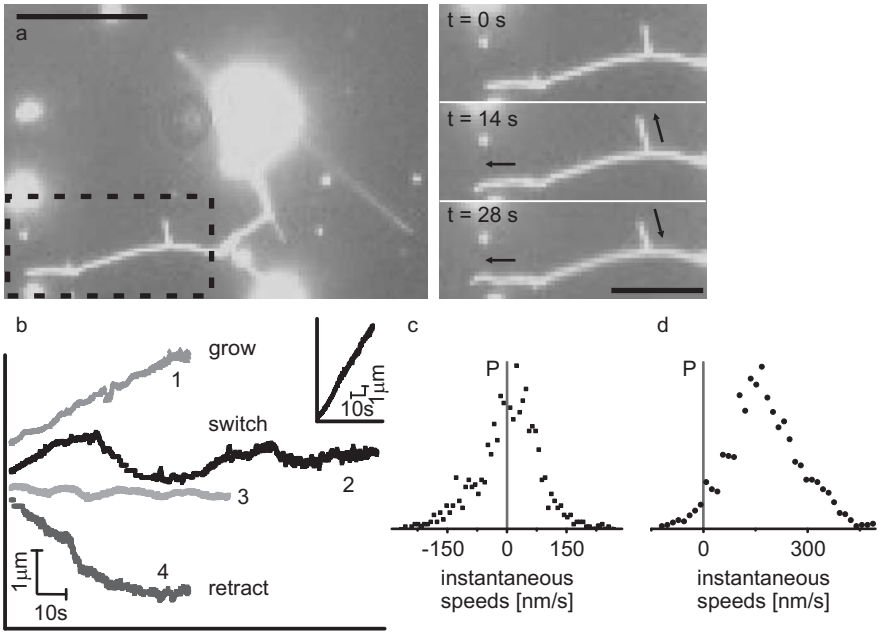

Figure 7.1: Membrane tubes formed by nonprocessive motors. (a) Fluorescence image of a membrane tube network extracted from GUVs by nonprocessive motors walking on MTs on the underlying surface. The time sequence images on the right show the detailed evolution of the network section within the dashed region on the left. The entire movie can be found in the supplementary material of [30]. Arrows indicate direction of membrane tube movement: the left arrows indicate a growing tube and the right arrows show a tube that which is switching between growth and retraction (left scalebar, $10\ \mu\mathrm{m}$, right scalebar, $5\ \mu\mathrm{m}$). (b) Example traces of membrane tube tips formed by nonprocessive motors as they move in time. There are three distinct behaviors: tube growth (1), tube retraction (4) and switching between growth and retraction (2 and 3), a bidirectional behavior. The behavior is distinctly different for membrane tubes pulled by Kinesin (inset) where tubes grow at steady high speeds. (c) The distribution of instantaneous tip speeds for membrane tubes pulled by Ncd is asymmetric and centers around zero, with both positive and negative speeds. (d) The distribution of instantaneous tip speeds for membrane tubes pulled by Kinesin is symmetric around a nonzero positive value, and does not include negative speeds.

7.2 Experimental results

The results in this section are from the experiments by P. M. Shaklee. Details on the experiments are given in appendix 7.A and [133]. We investigate the influence of motor properties on membrane tube pulling with a minimal system where biotinylated motor proteins are linked directly via streptavidin to a fraction of biotinylated lipids in GUVs. Upon sedimentation to a MT-coated surface, and addition of ATP, motors extract membrane tubes from the GUVs. These membrane tubes form networks, which follow the pattern of MTs on the substrate. Tubes and networks are formed in experiments with Kinesin motors [25] as well as in experiments with Ncd motors [30]. Figure 7.1a shows a fluorescence time series of membrane tubes pulled from a GUV by Ncd motors. The entire movie can be found in the supplementary material of [30]. The motion of the tip of a membrane tube being pulled by Ncd shows remarkable variability. The arrow on the lower right hand corner of the image of figure 7.1a indicates a retracting membrane tube and the remaining arrows show growing membrane tubes. Moreover, in the experiments we find not only tubes that persistently grow or retract, but also tubes that switch from periods of forward growth to retraction. We characterize these tube dynamics by tracing the tube tip location as it changes in time. Figure 7.1b shows example traces of Ncd-pulled membrane tube tips in time: one of tube growth, one of retraction and two that exhibit a bidirectional movement. We verify that this bidirectional tube movement is unique to nonprocessive motors by comparing to membrane tubes pulled by processive motors. Under the same experimental conditions Kinesins produce only growing tubes (figure 7.1b inset). In the rare cases of tube retraction with Kinesin, tubes snap back long distances at high speeds, at least 10 times faster than growth speeds. In these cases, it is likely that the motors pulling the tube have walked off the end of the underlying MT.

We further quantify membrane tube dynamics by calculating instantaneous speeds for individual tip traces by subtracting endpoint positions of a window moving along the trace. As described in appendix 7.A, we use a window size of $1\ \mathrm{s}$ for the Ncd, and $2\ \mathrm{s}$ for the Kinesin membrane tube tip traces. Figure 7.1c shows an example of the resulting distribution and frequency of tip speeds for a single dynamically switching membrane tube formed by Ncd (trace 2 from figure 7.1b). Figure 7.1d shows the speeds for a membrane tube pulled by Kinesin. The speed distributions for Kinesin and Ncd are distinctly different. Kinesin speeds show a Gaussian distribution around a high positive speed. From gliding assays, one expects that Kinesin would pull membrane tubes at approximately $500\ \mathrm{nm/s}$. The Kinesin motors along the bulk of the membrane tube are moving freely in a fluid lipid bilayer, do not feel any force and may walk at maximum speed toward the membrane tube tip. However, the motors at the tip experience the load of the membrane tube and their speeds are damped [25, 26, 134]. The Gaussian distribution of speeds we find for Kinesin elucidates the influence of load on the cluster of motors accumulating

at the tip of the membrane tube. The distribution of speeds for Ncd is asymmetric and centered around zero with both positive and negative speeds. A simple damping of motor walking speed at the membrane tip, as in the case of Kinesin, does not provide an explanation for the distribution of negative membrane tube speeds found in the tubes pulled by Ncd. The unique tube pulling profile of the nonprocessive motors suggests that they provide a mechanism to mediate membrane retractions and hence, bidirectional tube dynamics.

7.3 Model

Koster *et al.* [25] showed that membrane tubes can be formed as a result of motors dynamically associating at the tube tip. Collectively, the clustered motors can exert a force large enough to pull a tube. Evans *et al.* [45, 46] found that this force scales as $\mathcal{F}_{\text{tube}} \sim \sqrt{\kappa\sigma}$, where κ is the membrane bending modulus and σ the surface tension (see section 2.3.5). Koster *et al.* predicted a stable tip cluster to pull a tube, which has been verified experimentally by Leduc *et al.* [26] and supported by a microscopic model by Campàs *et al.* [28].

Although accurate for membrane tubes produced by processive motors, the Kinesin model does not explain the bidirectionality in tubes formed by nonprocessive motors. There must be an additional regulatory mechanism for the tube retractions to explain the negative speed profiles seen in experiments with Ncd. We propose a mechanism to account for these retractions wherein dynamic clusters form along the entire length of the tube. In the case of Kinesin, motors walk faster than the speed at which the tube is pulled, and accumulate at the tip cluster [25, 26]. However, in the case of Ncd the situation is completely different. Because they are nonprocessive, these motors simply can not walk to the tip of the membrane tube. Moreover, once bound, it takes a long time before they take a step and unbind again. Compared to freely diffusing motors ($D = 1\ \mu\text{m}^2/\text{s}$ [26]), a MT-bound motor (bound for approximately $0.1\ \text{s}$ [22, 136]) is therefore effectively stationary. Consequently, there are MT-bound motors all along the length of the tube. Local density fluctuations (and possibly cooperative binding [137]) lead to areas of higher concentration of bound motors, resulting in the formation of many motor clusters, not just a single cluster at the tube tip.

In both cases, the cluster present at the tip has to be large enough to overcome $\mathcal{F}_{\text{tube}}$. Because an individual motor can provide a force up to approximately $5\ \text{pN}$ [128] and a typical $\mathcal{F}_{\text{tube}}$ is $25\ \text{pN}$ [25], a cluster must consist of at least several motors to sustain tube pulling. Statistical fluctuations can make the tip cluster too small to overcome $\mathcal{F}_{\text{tube}}$, resulting in a retraction event. In the case of Ncd, as soon as the retracting tip reaches one of the clusters in the bulk, the tube is caught, and the retraction stops. Growth can then resume, or another retraction event takes place. The process of clustering along the membrane tube, as illustrated in figure 7.2, and the associated rescue mechanism

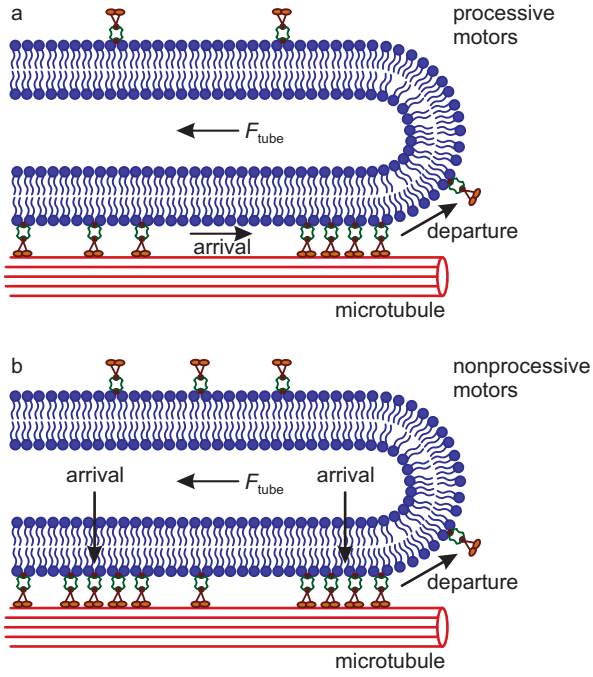

Figure 7.2: Sketch of the pulling of a membrane tube by a cluster of molecular motors. (a) Pulling by a cluster of processive Kinesin motors. Motors can bind to the microtubule anywhere along the membrane tube. Because the bound motors along the tube do not experience a load, they catch up with the cluster of motors at the tip, which thus gets replenished continuously. The only cluster is the tip cluster which pulls the tube; motors occasionally unbind from this cluster. (b) Pulling by a cluster of nonprocessive Ncd motors. Here too, motors can bind to the microtubule anywhere along the membrane tube. Since the motors can not walk continually towards the tip, they do not replenish the tip cluster. However, because Ncd motors stay bound for a long time, random density fluctuations cause clusters to appear anywhere along the membrane tube. The tip cluster can only be replenished by motors binding near or at the tip and is therefore small. If the number of motors in the tip cluster becomes too small to withstand the tube tension, a retraction event occurs, in which the tube snaps back rapidly to the next cluster.

are absent from the mechanism that describes Kinesin tube pulling. There, however, the tip cluster is typically very large (30-50 motors [25]), so fluctuations large enough to make it disappear are very rare.

In our model for pulling by Ncd motors two different mechanisms drive forward and backward tube motion, so we expect two different types of characteristic motion profiles. Retraction is regulated by motor clusters that can form anywhere along the length of the tube: their locations are randomly taken from a uniform probability distribution. Consequently the distance between them follows an exponential distribution. The long steptime of MT-bound Ncd motors allows us to temporally resolve the effect of the disappearance of clusters from the tube tip: individual retraction events. We therefore expect to recover this exponential distribution in the retraction distances.

The forward velocity depends on the size of the cluster at the tube tip, in agreement with the results from the gliding assay experiments [130]. Per experimental timestep there are many motors arriving at and departing from each cluster. Moreover, while taking a time trace we observe pulling by several different clusters of motors. Because there are many clusters in an individual trace, we can employ the Central Limit Theorem to approximate the distribution of cluster sizes by a Gaussian. If the number of motors in the tip cluster is large enough to overcome the tube force, the speed at which the cluster pulls scales with the number of excess motors: $v = A(n-c)$, up to a saturation point (typically at a cluster size of about 12 motors [130]). Here n is the number of motors, c the critical cluster size and A the scaling constant that depends on the turnover rate, stepsize and tube tension. The forward speed distribution will therefore inherit the Gaussian profile of the cluster size distribution, where the mean and spread of this distribution depend on the average tip cluster size. The probability density of the exponential distribution function depends on a single parameter λ, the mean retraction distance. The Gaussian distribution depends on both the mean $\langle n \rangle$ and the spread σ_n of the tip cluster.

The tube dynamics are described by the probability distribution of the tip displacement per unit time. From the individual probability densities for retraction and growth we find the combined density $f(\Delta L)$, the full probability density of advancing or retracting a distance ΔL:

$$f(\Delta L) = \begin{cases} (1-Z)\frac{1}{\lambda}\exp\left(-\frac{|\Delta L|}{\lambda}\right) & \Delta L < 0 \\ & \text{(retract)} \\ \frac{1}{\sigma_n\sqrt{2\pi}}\exp\left[-\frac{1}{2}\left(\frac{(\Delta L/s)-(\langle n\rangle - c)}{\sigma_n}\right)^2\right] & \Delta L \geq 0 \\ & \text{(advance)} \end{cases} \tag{7.1}$$

where n is the size of the cluster at the tip, c is the minimal cluster size necessary to support the tube, and s the steplength, which is equal to the size of a MT subunit (8 nm) [130]. The normalization constant Z depends on $\bar{n} = \langle n \rangle - c$

and σ_n and is given by

$$Z = \frac{1}{2}\left[1 + \mathrm{erf}\left(\frac{\bar{n}}{\sigma_n\sqrt{2}}\right)\right]. \tag{7.2}$$

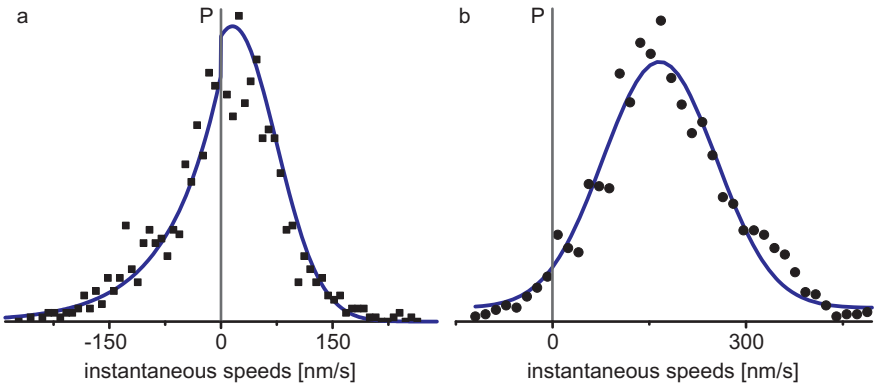

Figure 7.3: Distribution of instantaneous speeds of the tip of a membrane tube pulled by molecular motors. (a) Tip speed distribution of a tube pulled by nonprocessive Ncd motors, resulting in a a bidirectionally moving membrane tube (trace 2 in figure 7.1b). The speed distribution can be described as a combination of two different processes: pulling by nonprocessive motors and tube tension induced retraction. Therefore the forward and backward speeds follow different distributions, as described by equation (7.1); the solid line shows the best fit of this distribution. (b) Tip speed distribution of a tube pulled by processive Kinesin motors, resulting in a tube growing at constant speed (inset in figure 7.1b). The speed distribution can be described by a Gaussian (best fit shown as a solid line), indicating that there is always a cluster present at the tip to pull the tube forward.

7.4 Phase diagram

From the experimental data we cannot determine $\langle n\rangle$ and c individually, but only speed profiles which scale with the difference $\bar{n} = \langle n\rangle - c$, the number of excess motors present in the tip cluster that actually pull. To determine $A\bar{n}$, $A\sigma_n$ and λ, we make use of the fact that Z is the fraction of forward motions, providing a relation between $\bar{n}$ and σ_n. We then have a two-parameter fit for the entire speed distribution, or two single-parameter fits for the forward and backward parts of the total speed distribution.

We apply our model to experimental data and find that the different mechanisms for forward and backward motion accurately describe the experimental Ncd tip traces (figure 7.3a). As predicted, Kinesin motors only show forward pulling speeds, described by a Gaussian distribution (figure 7.3b). The marked contrast in speed profiles of processive and nonprocessive motors is a signature of different biophysical processes: for processive motors a single cluster remains at the tip ensuring a constant forward motion whereas tubes pulled by nonprocessive motors are subject to alternating growth and retraction phases.

Growth and retraction are accounted for by the two different mechanisms in our model. Combined, they explain the three different types of observed behavior: growth, retraction, and switching between these. To unravel the relationship between the two mechanisms in describing membrane tube behavior, we plot the characteristic growth rate $A\bar{n}$ versus the characteristic retraction length λ in a 'phase diagram'. Because a trace exhibiting switching behavior should have an average displacement of zero, we can derive a 'switching condition' from the probability distribution (7.1) by requiring the expectation value of ΔL to vanish. The line in the phase diagram where this switching condition is met is given by:

$$\lambda_s = A\bar{n}\frac{Z}{1-Z} + \frac{A\sigma_n}{\sqrt{2\pi}}\frac{1}{1-Z}\exp\left[-\frac{1}{2}\left(\frac{\bar{n}}{\sigma_n}\right)^2\right] \tag{7.3}$$

where Z is the normalization constant given by equation (7.2). In figure 7.4a we plot the lines for which the switching condition holds for the range of values for $A\sigma_n$ we find in the experimental traces ($50\,\mathrm{nm/s} \leq A\sigma_n \leq 70\,\mathrm{nm/s}$). We also plot the experimentally obtained values for $A\bar{n}$ and λ of the four traces given in figure 7.1b. We clearly see different regimes. Growing tubes have large average cluster size and small distances between clusters. Retracting tubes show the inverse characteristics (small cluster size and large distance between clusters). The switching tubes are in between, in a relatively narrow region.

7.5 Simulations

The switching regime covers only a small part of the total available parameter regime in the phase diagram (see figure 7.4a). That we observe switching behavior in approximately $50\ \%$ of the experimental traces indicates that these parameters are dynamic quantities that change over time. Our experimental observation times are too short to track these changes, but we can implement them in simulations. When introducing dynamics into our model, it is important to realize that the tube force $\mathcal{F}_{\text{tube}}$ is not independent of the tube length, an additional observation not yet integrated into the model. As tubes grow longer the vesicle itself starts to deform. Consequently, the tube force increases with the tube length, an effect also observed experimentally [138].

The force exerted by a single motor is constant, so a larger force requires more motors to pull at the same time for a tube to grow. A length-dependent pulling force therefore naturally leads to a typical lengthscale L_c, on which the force exerted by an average tip cluster exactly balances the force exerted by the tension in the tube. Rather than to explicitly introduce a force into our system, we model the length-dependence by rescaling the number of motors available for pulling. We do so by introducing an exponential factor that compares the length of the tube to the lengthscale L_c. The number of motors on the entire tube as a function of time is then given by

$$N(t) = C2\pi R_0 L(t) e^{-L(t)/L_c}, \tag{7.4}$$

where C is the average motor concentration on the GUV and R_0 is the tube radius.

Combined, equations (7.1) and (7.4) form a dynamical system which describes the time-dependent membrane tube behavior when pulled by nonprocessive motors. We simulate that system with values for C and R_0 from the experimental data. In the simulations, we assume that tubes are initially pulled from motor-rich regions on the GUV; this assumption is not necessary but helps to get the pulling process started, while limiting the retraction distances. As a tube grows longer, clusters are spread further apart and the average cluster size decreases. The average retraction distance increases with increasing tube length, $L(t)$, and scales inversely with the total number of motors, $N(t)$, on the tube: $\lambda \sim L(t)/N(t)$. Similarly, the average number of motors at the tip scales with the total number of motors $N(t)$ and inversely with the tube length $L(t)$: $\langle n \rangle \sim N(t)/L(t)$. We choose the simulation timestep to match the experimental sampling rate of 25 Hz. In each timestep we add Gaussian noise to the position of the tip to account for the experimental noise. In the simulations we observe two kinds of behavior: tubes that grow and subsequently retract completely after relatively short times, and tubes that evolve to a switching state. In control simulations where the exponential factor in equation (7.4) is left out, we find either fully retracting or continuously growing membrane tubes, never switching.

Figure 7.4b shows two examples of simulated switching traces. We follow the average number of motors at the tip $\langle n \rangle$ and the retraction distance λ as they change in time. The simulated evolution from growth to a switching state can be seen in the phase diagram shown in figure 7.4a. In the switching state, the tube length and total number of motors on the tube are essentially constant, and equation (7.3) is satisfied.

The highlighted sections of the simulated traces shown in figure 7.4b represent all possible characteristic behaviors of tubes pulled by nonprocessive motors. The occurrence of all three types of behavior in a long simulated tube tip trace suggests that the experimental observations are snapshots of a single evolving process. The simulations indicate that all these processes eventually move to the switching regime. The switching state is therefore a dynamic

attractor of this system. The position of the attractor in the phase diagram corresponds to a regulated tube length, determined by the GUV's motor concentration and surface tension.

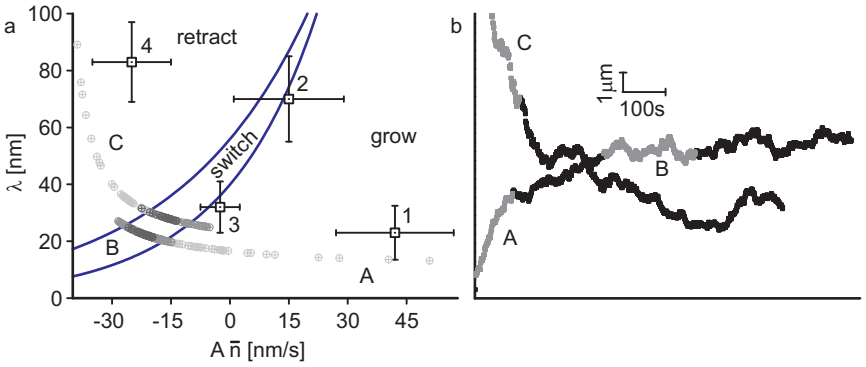

Figure 7.4: Membrane tube phase diagram and simulations. (a) Phase diagram showing mean retraction distance λ vs. effective growth speed $A\bar{n}$. Lines represent the switching condition described by equation (7.3) for $A\sigma_n = 50\ \mathrm{nm/s}$ and $A\sigma_n = 70\ \mathrm{nm/s}$. Squares 1-4 correspond to traces 1-4 in figure 7.1b, where the errors are determined by the mean square difference between the data points and the fit of distribution (7.1). As expected qualitatively, retracting membrane tubes fall well into the retraction regime with large retraction distance and small cluster sizes, while growing membrane tubes have large cluster sizes and smaller distances between clusters. (b) Two simulated tube tip traces of a membrane tube pulled by nonprocessive motors. The time evolution of the parameters λ and $A\bar{n}$ for both traces is shown in the phase diagram (a), by circles getting darker in time. We find that both simulated tubes evolve towards a switching state. The highlighted sections (A, B, C) of the simulated traces represent all possible characteristic behaviors of tubes pulled by nonprocessive motors.

7.6 Conclusion

Both processive and nonprocessive motors can collectively pull tubes from membrane vesicles. Tubes pulled by processive motors are growing at a constant speed. On the other hand, tubes pulled by nonprocessive motors exhibit a variety of speeds and even bidirectionality in their motion. Two different mechanisms are involved in producing this bidirectional behavior: pulling by motors and retraction by tension. We captured both mechanisms in a single

model. In this model motors spontaneously organize into clusters due to random fluctuations in motor density. The cluster at the tip is responsible for the forward motion and the backward motion originates from the tube retracting to the next stable motor cluster. Our model predicts the emergence of a dynamic attractor at an equilibrium tube length where bistability occurs, in agreement with the experimental observations.

7.A Experiments

The experimental data given in chapter 7 were obtained by P. M. Shaklee from the Leiden experimental biophysics group and AMOLF, and are used here with permission. In this appendix we briefly sketch the experimental procedure for obtaining the experimental data shown in figures 7.1, 7.3 and 7.4. More details can be found in [133].

The Giant Unilamellar Vesicles (GUVs) used in the tube pulling experiments consist primarily of DOPC lipids. To visualize them, a small amount of fluorescent Rhodamine lipid is included in the membrane bilayer. Moreover, to provide for binding sites for the molecular motors, a small amount of biotin lipids is included as well. GUVs are prepared in such a way that there is no osmotic pressure gradient across their membrane. After formation of the GUVs, $2\,\mathrm{mg/ml}$ streptavidin is added to 50 μl of vesicle solution. The streptavidin acts as a linker between the biotin lipids in the GUVs and the motors; the quantity of streptavidin added is chosen such that all biotin binding sites on the vesicles are saturated. Finally $2\ \mu\mathrm{l}$ of motor solution (Kinesin or Ncd, $\sim 650\ \mu\mathrm{g/ml}$) is added and incubated for 10 minutes, allowing all motors from the solution to bind to available biotin-streptavidin complexes.

Microtubules (MTs) are prepared from tubulin dimers, the MT building blocks consisting of an α and a β tubulin protein. The MTs are allowed to polymerize in a buffer solution for 15 minutes at $37^{\circ}\mathrm{C}$, and subsequently stabilized by adding $10\ \mu\mathrm{M}$ taxol protein. The solution containing the stabilized MTs is dropped on a prepared glass coverslip, where they are incubated for 10 minutes to adhere. MTs that do not stick to the surface are removed by rising twice with a buffer solution. Finally the surface is coated with α-Casein protein.

The Kinesin motors used are the first 401 residues of the Kinesin-1 heavy-chain from *Drosophila melanogaster*, with a hemaglutinin tag and a biotin at the N-terminus. To produce them, they are expressed in *Escherichia coli* and purified as described in [139]. The Ncd motors are the residues K195-K685 of the nonclaret disjunctional (Ncd) from *Drosophila melanogaster*, with a 6x-His tag [136] and biotin. They are expressed and purified in the same fashion as the Kinesins.

In the experiments $40\ \mu\mathrm{l}$ of the vesicle solution (containing GUVs with attached motors) is dropped on top of the glass coverslips decorated with the stabilized MTs. A saturating solution of $1\ \mu\mathrm{l}\ 100\ \mathrm{mM}$ ATP is added to provide

the fuel source for the motors.

Images are acquired on an epifluorescence inverted microscope equipped with a CCD camera at videorate. We developed a Matlab® algorithm to trace the membrane tube growth dynamics by following the tip displacement as a function of time. The algorithm determines the intensity profile along a tube and extended beyond the tip. A sigmoidal curve fit to the profile to determines the tip location with subpixel precision of $40\ \mathrm{nm}$. We traced tip locations for 7 individual Kinesin-pulled membrane tubes (all growing, a single one showing a rapid retraction event) and 15 Ncd tubes (5 growing, 3 retracting, and 7 switching). We calculated instantaneous speeds for individual tip traces by subtracting endpoint positions of a window moving along the trace. Initially we used a range of window sizes, from $0.5\ \mathrm{s}$ to $12\ \mathrm{s}$, to calculate instantaneous speeds from the tip traces. We found that, for the Ncd data, a window size of $1\ \mathrm{s}$ is large enough to average out experimental system noise (signal due to thermal noise, fluorophore bleaching and microscope stage drift) but small enough to preserve the unique bidirectional features we see in tube data. Windows of 2 and $3\ \mathrm{s}$ begin to overaverage the data, and even larger window sizes smooth away the prevalent changes in speeds and directionality already qualitatively evident in the data. For Kinesin, however, the resulting speeds we found using a window size of $2\ \mathrm{s}$ (minimum size for the Kinesin data, the experimental signal is noisier than for the Ncd data) differ very little from the speeds we get using up to an $8\ \mathrm{s}$ window. Ultimately, we used small window sizes that are still large enough to average out experimental noise but preserve as much of the signal details as possible: $1\ \mathrm{s}$ for Ncd tip traces and $2\ \mathrm{s}$ for Kinesin traces, with steps of $0.04\ \mathrm{s}$. We determined the noise in our system (signal due to thermal noise, fluorophore bleaching and microscope stage drift) by analyzing stationary membrane tubes with our tip-tracing algorithm and calculating instantaneous speeds in the same fashion as for active tube tips. The speeds from a noise trace showed a Gaussian profile centered around zero with a spread of $40\ \mathrm{nm/s}$.